ACS EARTH AND SPACE CHEMISTRY

http://pubs.acs.org/journal/aesccq
Article

Propyne: Determination of Physical Properties and Unit Cell Parameters under Titan-Relevant Conditions

Theresa C. Marlin,* Morgan L. Cable, Tuan H. Vu, Helen E. Maynard-Casely, Melissa Ugelow, Carrie Anderson, and Robert Hodyss

Cite This: *ACS Earth Space Chem.* 2024, 8, 957−964

ABSTRACT: With its large size, dense atmosphere, methane-based hydrological-like cycle, and diverse surface features, the Saturnian moon Titan is one of the most unique of the outer Solar System satellites. Study of the photochemically produced molecules in Titan's atmosphere is critical in order to understand the mechanics of the atmosphere and, by extension, the interactions between atmosphere, surface, and subsurface water ocean. One example is propyne vapor, a photochemically produced species in Titan's upper atmosphere expected to condense in Titan's stratosphere at lower altitudes. Propyne may also be a trace species in Titan's stratospheric co-condensed ice clouds detected by the Cassini Composite InfraRed Spectrometer. Bulk structural characterization of propyne ice is currently incomplete and is lacking in published laboratory Raman spectra and X-ray diffraction data. Here, we present a laboratory characterization of propyne ice, including the first published X-ray diffraction and Raman spectroscopy results for propyne ice.

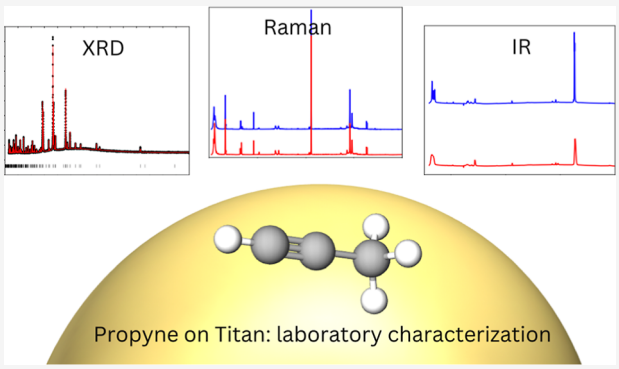

KEYWORDS: *propyne, ice, Raman, crystalline, amorphous, infrared, spectroscopy, X-ray diffraction*

INTRODUCTION

Complex photochemistry in the upper atmosphere of Saturn's moon Titan produces a variety of hydrocarbon, nitrile, and other species with varying distributions throughout the moon's thick atmosphere.[1−3] Among these species, propyne (methylacetylene; $HC{\equiv}C{-}CH_3$) vapor is formed in Titan's upper atmosphere via the following reactions:[4]

formation of allene, propyne's isomer:

$$CH + C_2H_4 \rightarrow CH_2CCH_2 + H \quad (1)$$

H exchange reaction to form propyne:

$$H + CH_2CCH_2 \rightarrow H + CH_3CCH \quad (2)$$

alternative reaction to form propyne:

$$H + C_3H_3 + M^* \rightarrow CH_3CCH + M \quad (3)$$

recombination reaction:

$$H + CH_3CCH + M \rightarrow C_3H_5 + M \quad (4)$$

degradation by photolysis:

$$C_3H_4 + h\nu \rightarrow C_3H_3 + H \quad (5)$$

*: M denotes a neutral body (e.g., N_2) that is required for energy balance in the termolecular reactions.

Propyne gas was first detected in Titan's stratosphere by the InfraRed Interferometer Spectrometer (IRIS) onboard the *Voyager* 1 spacecraft in 1981, where the spacecraft passed by Titan shortly after northern spring equinox.[5] Nearly one Saturnian year later, the arrival of the *Cassini* spacecraft allowed further observations of these gas species at an analogous time in Titan's seasonal cycle.

Propyne's abundance and distribution in Titan's atmosphere undergo seasonal variation. Titan is predicted to have one pole-to-pole global atmospheric circulation cell with upwelling at the summer pole and subsiding at the winter pole.[6] Photochemical trace species abundance in Titan's atmosphere is correlated with the satellite's seasons, with increased enrichment occurring at the winter pole as the global circulation cell carries them from the upper stratosphere.[7] The atmospheric distribution of propyne was studied contemporaneously with *Cassini* and the Atacama Large Millimeter/submillimeter Array (ALMA). Prior to northern spring equinox, propyne abundance was enriched in the

Received: October 31, 2023
Revised: January 22, 2024
Accepted: January 23, 2024
Published: April 16, 2024

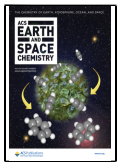

https://doi.org/10.1021/acsearthspacechem.3c00303
ACS Earth Space Chem. 2024, 8, 957−964

north.[8] ALMA observations in 2012 (shortly after northern spring equinox) revealed a sustained presence of propyne in the northern regions as well as several other photochemically produced trace species.[9] It was theorized that these species were left over from northern winter, when they had been deposited by the reversed global circulation cell and were undergoing slow photochemical destruction. Data from 2010 to 2015 taken by the *Cassini* Composite InfraRed Spectrometer (CIRS) shows the abundance of propyne steadily increasing at southern polar latitudes as the pole transitions into winter.[10] The southern increase of propyne abundance was separately confirmed with ALMA data.[11] While the enrichment of trace species in southern regions was detectable shortly (several earth years) after equinox, the decrease in trace species in the north was not widespread until six earth years post-equinox.[12] Even then, propyne persisted in the north: data collected five to seven years after equinox revealed constant amounts of propyne in Titan's mid-northern latitudes.[13] However, its vertical distribution does experience shorter-scale seasonal variation, steepening as the northern hemisphere passes into spring.[14,15] Despite the prevalence of propyne vapor in Titan's atmosphere throughout a Titan year, pure stratospheric propyne ice has not yet been detected.

It is possible that propyne ice is instead a component of the mixed-organic clouds. The *Cassini* CIRS instrument also identified a number of distinct stratospheric clouds, particularly near the winter pole.[16] With the rich diversity of photochemically produced trace species present in Titan's atmosphere, there are a wide range of potential compositional profiles for these clouds, many of which are thought to be formed by co-condensed trace species.[16] The saturation vapor pressure curve for propyne intersects the constructed pressure−temperature profile of Titan's atmosphere (based on July 2015 data at 79° south) at an altitude of approximately 70 km, indicating that propyne may be a viable component of stratospheric clouds on Titan.[16] However, co-condensation leads to varied optical properties; a co-condensate of trace species does not necessarily have strictly the additive spectral characteristics of its constituents; it can have spectral features that do not result from any linear combination of its pure components.[16]

Organic ice particles formed in the stratosphere, such as propyne, slowly drift downward. They eventually make their way to the troposphere and are theorized to deposit on Titan's organic-laden surface.[16] The deposition rate of propyne onto the surface can be calculated based on modeled condensation flux.[4] The condensation flux of propyne in Titan's atmosphere has been calculated in several models, but wide variation exists among these values. Krasnopolsky (2009), Lara et al. (1996), and Yung et al. (1984) have predicted column-integrated condensation fluxes of 2.6×10^6 molecules/(cm^2·s), 1.1×10^4 molecules/(cm^2·s), and 5.7×10^7 molecules/(cm^2·s), respectively, which (assuming a density of 1000 kg/m^3) corresponds to a propyne deposition rate of 0.23−1200 μm/Myr on Titan's surface.[17−19] Once deposited, propyne may interact with other organic species to form surface co-crystals or other cryominerals, as has been experimentally demonstrated to be feasible with other abundant and trace species in Titan-relevant conditions.[3,20−22] Co-crystal formation is proposed on Titan via either interactions between photochemical surface deposits and liquid hydrocarbon regions or via solid-state chemistry.[23]

Before propyne's behavior as a co-condensate in stratospheric ice clouds or as a component of a surface co-crystal can be fully understood, pure propyne ice must be fully characterized under Titan-relevant conditions. Additionally, we conducted experiments on pure propyne in conditions that were not Titan-relevant in order to deepen the overall understanding of the chemical and physical properties of this molecular solid. Laboratory characterization of propyne to date has been minimal, with only three laboratory studies found in the literature.[24−26] The two studies published in 1940 and 1983 contain Raman spectra for propyne in liquid and gas phases as well as the infrared spectrum for the gas phase[24,25] (1940: ∼300 to ∼3300 cm^{-1}; 1983: 100 to 3400 cm^{-1}; temperature and pressure were not specified). The third study in 2021 was recently published, reporting an infrared temperature series of propyne ice, T_{min} = 8 K, under ultrahigh vacuum (500 to 3600 cm^{-1});[26] but to the best of our knowledge, no complementary Raman spectra have been published for solid propyne. Raman spectroscopy provides a powerful tool for bulk structural ice characterization and the identification of phases. Here, we report X-ray diffraction data (collected between 1.5 and 8.5 Å), solid phase Raman spectra (50 to 4000 cm^{-1}), and infrared spectra (600 to 4000 cm^{-1}) in conditions relevant to Titan's atmosphere. To the best of our knowledge, X-ray diffraction data and solid-phase Raman data of propyne have not been made publicly available prior to this work. Our data provide broad qualitative information about bulk structural properties of propyne and provide a foundation for the chemical and physical behaviors of this molecule.

EXPERIMENTAL METHODS

The experimental methods used to gather X-ray diffraction (XRD), Raman, and Infrared (IR) data are described below. Note that none of our methods employed unusually dangerous or hazardous components.

X-ray Diffraction. To gain insights into the bulk structural characteristics of solid propyne, a synchrotron powder diffraction experiment was carried out using the mail-in program at Argonne National Laboratory's Advanced Photon Source (APS) 11-BM beamline. Propyne gas was first condensed via a vacuum manifold into a 0.9 mm borosilicate capillary (Charles Supper Co., Inc.) submerged under liquid nitrogen. While propyne was still frozen, a butane torch was used to flame cut and seal the capillary tube at the appropriate length for the provided sample container. The tube was then allowed to warm up to room temperature, where the propyne melts and equilibrates with its vapor pressure in the headspace (∼5 bar). After confirmation that the capillary can withstand this pressure for several days, it was then inserted into a Kapton sleeve and mounted onto the provided sample base and covered by a magnetic cap. Afterward, the sample was shipped to the APS facility, where it was frozen at 90 K and diffraction patterns acquired at various temperatures (90, 100, 120, 140, and 160 K) over the allocated beam time of 8 h. The incident X-ray beam for these collections was λ = 0.458155 Å, with a multianalyzer detection system also used for all data collections.

The synchrotron data were supplemented with experiments prepared in a similar manner using a laboratory Bruker D8 DISCOVER DaVinci instrument. This instrument is equipped with a Cu Kα X-ray source (λ = 1.5406 Å), a linear energy-dispersive LynxEye XE-T 1D detector, and an Oxford Cryosystems 800 cryostream for temperature control to within ±1 K. Here, a capillary containing liquid propyne was first frozen at 85 K, followed by incremental increases in

https://doi.org/10.1021/acsearthspacechem.3c00303
ACS Earth Space Chem. 2024, 8, 957−964

temperature every 5 K until 120 K. Diffraction patterns were recorded at each temperature point for ∼1 h over the 2θ range of 10−60° (angular resolution of 0.02°). Refinements of all experimental patterns from both the synchrotron and laboratory data were undertaken using the Topas suite (version 6).[27]

Raman. Raman spectra were collected using a high-resolution confocal dispersive micro-Raman spectrometer (Horiba Jobin Yvon LabRam HR), equipped with a 532 nm laser operating at 50 mW, an 1800 grooves/mm diffraction grating, and a 50× Olympus BXFM objective. The system utilized an Oxford MicroStatN liquid nitrogen-cooled vacuum cryostage mounted to the *XYZ* motorized translation stage underneath the objective turret; the cryostage is capable of reaching temperatures as low as 75 ± 0.5 K. Deposition of the propyne onto the sample plate was conducted through a 1/16 in. stainless steel tube to control where the deposition occurred. The obtained Raman spectra cover the 50−4000 cm^{-1} frequency range at a 0.4 cm^{-1}/px resolution. The silicon 520.7 cm^{-1} peak was used for frequency calibration. Between two and four spectral accumulations were obtained per final spectrum in order to improve the signal-to-noise ratio.

Multiple temperature dependence studies were conducted. In the first, propyne (Aldrich, >97% purity) was deposited from the gas phase into the cryostage at the lower temperature limit of the system, 75 K. Raman spectra were collected in 5 K increments from 75 to 120 K (with an equilibration time of 5 min at each temperature point). The converse of this experiment was also conducted, with deposition at 120 K followed by cooling in 5 K increments (with the same equilibration time) and corresponding spectral collection until the lower temperature limit of the system was reached. A third experiment was performed in which propyne was condensed at a midpoint of 105 K.

Infrared. The experimental apparatus used for the acquisition of infrared spectra has been described elsewhere.[28−30] Briefly, propyne ice films were deposited at 15 K on a CsI window cooled by a closed cycle He refrigerator (ARS 202B) at a rate of 4.5 μm/h. The temperature of the window was controlled with a resistive heater and monitored with a Si diode thermometer (DT-670, ±0.5 K) affixed to the copper window frame. The thickness of the ice film was monitored during growth by laser interferometry (laser wavelength = 637 nm, laser/detector angle ∼5°) and was approximately 0.6 μm using an n_0 from the literature that was measured at 15 K and 670 nm (n_0 = 1.370).[26]

The window is contained within an ultrahigh vacuum system that routinely reaches a base pressure less than 5×10^{-10} Torr. Gas samples are introduced into the vacuum chamber through a separate turbopumped line with a base pressure of no more than 1×10^{-6} Torr. The flow of gas into the chamber is regulated with a precision leak valve (VACGEN, LVM Series). The gas enters the chamber through a 1/16 in. diameter stainless-steel tube directed at the deposition window, whose tip is approximately 5 cm from the deposition window. Propyne was used without further purification. No evidence of contaminants was observed in the resultant spectra for propyne.

IR spectra were recorded in transmission with a Nicolet 6700 FTIR spectrometer, at a resolution of 2 cm^{-1} full width at half-maximum. Each spectrum ranged from 600 to 4000 cm^{-1} and is the result of 1000 coadded single scan spectra. Samples were equilibrated for 5 min at the temperature of interest before spectra were collected. Samples were collected in 10 K increments from 15 to 105 K, the latter temperature being the point at which propyne sublimated.

RESULTS

X-ray Diffraction. Figure 1 shows the diffraction pattern of propyne at 90 K obtained from the synchrotron experiment.

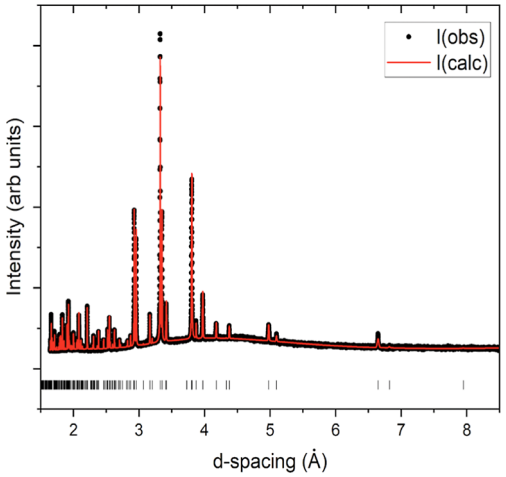

Figure 1. Pawley fit of the 90 K synchrotron diffraction data to the *Pbca* unit cell, a = 15.89410(11) Å, b = 13.2987(1) Å, and c = 5.7070(6) Å. Tick marks below the data indicate the expected positions of Bragg peaks from this unit cell. The fit of these data yielded R_{wp} = 8.46%, R_p = 6.21% with peaks described by a Thomson−Cox Hastings model and background by a 7-order Chebyshev polynomial (additional large-width peak included in the background to describe amorphous scattering from the silicate capillary).

Indexing of this pattern showed that the observed Bragg peaks could be fit with an orthorhombic unit cell with a = 15.89410(11) Å, b = 13.2987(1) Å and c = 5.7070(6) Å, resulting in a volume of 1206.30(2) $Å^3$. Fitting first with a *P*222 unit cell revealed a number of systematic absences (in 0*kl*, *h*0*l*, *hk*0, *h*00, 0*k*0, and 00*l* reflections) that supported the assignment of *Pbca* as the space group for this phase.

Figure 2 shows the laboratory XRD patterns of propyne as a function of temperature. A comparison with Figure 1 confirms that propyne adopts the same orthorhombic structure as in the synchrotron experiment and maintains this singular crystalline phase between 85 and 120 K. Using the determined *Pbca* space group, Pawley refinements are performed on each of the obtained experimental patterns (from both synchrotron and laboratory sources). The detailed lattice parameters as a function of the temperature are listed in Table 1. The relative expansion, where the values are normalized to those at the coldest temperature (85 K), is plotted in Figure 3.

Raman. At 125 K under low pressure, the propyne sublimated before a full spectrum could be collected. Thus, spectra for the vacuum series were collected in the range of 75 to 120 K. Deposition at 75 K yielded amorphous-phase propyne, while a deposition at 120 K was crystalline (Figure 4). When propyne was incrementally heated following deposition at 75 K, a gradual amorphous-to-crystalline phase transition appeared to occur between 105 and 107 K (Figure S1). Direct deposition at 105 K corresponded to a crystalline structure (Figure S2, purple/top trace), and subsequent cooling from a higher-temperature deposition yielded no

https://doi.org/10.1021/acsearthspacechem.3c00303
ACS Earth Space Chem. 2024, 8, 957−964

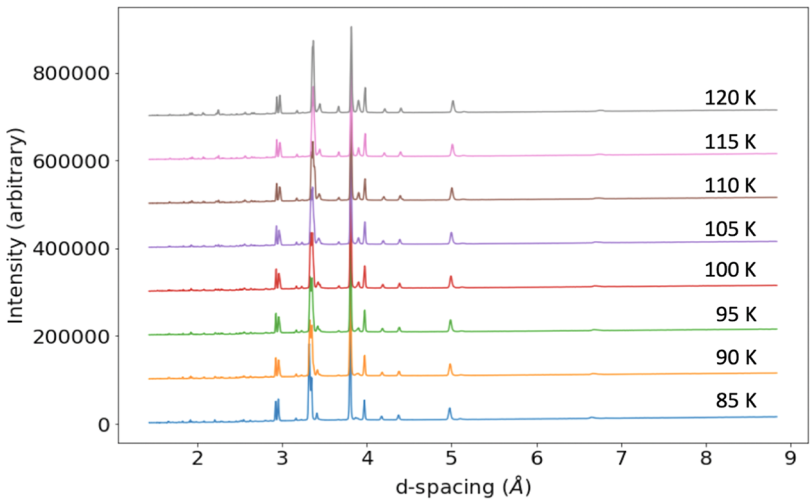

Figure 2. Diffraction patterns of propyne obtained on the laboratory X-ray source (λ = 1.5406 Å) as a function of temperatures. The sample was first frozen at 85 K, followed by an incremental temperature increase every 5 K.

Table 1. Lattice Constants and Unit Cell Volumes of Propyne over Its Temperature Stability Range of 1 bar[a]

temperature (K)	a (Å)	b (Å)	c (Å)	V (Å^3)
85	15.892(6)	13.287(4)	5.714(7)	1206.6
90	15.902(2)	13.314(7)	5.717(5)	1210.4
95	15.906(0)	13.325(0)	5.718(0)	1211.9
100	15.907(1)	13.342(2)	5.723(2)	1214.6
105	15.914(0)	13.364(0)	5.729(0)	1218.3
110	15.918(0)	13.390(0)	5.735(0)	1222.4
115	15.923(0)	13.418(0)	5.744(0)	1227.4
120	15.926(0)	13.432(0)	5.746(0)	1229.2
140	15.936(0)	13.500(0)	5.763(1)	1239.9
160	15.955(0)	13.573(3)	5.784(1)	1252.5

[a]Values were obtained from Pawley refinements.

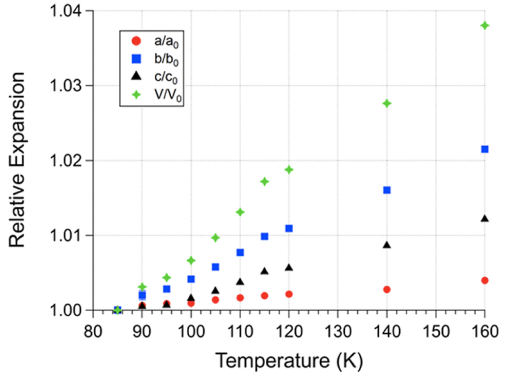

Figure 3. Thermal expansion of propyne as derived from Pawley refinements (Table 1). Lattice constants and unit cell volumes are normalized to those at the coldest temperature under study (85 K).

structural change as the propyne remained in the crystalline phase (Figure S3).

The difference between the crystalline and amorphous phases can be observed through differentiated features across the Raman spectra. The most diagnostic region of this transition is between 600 and 700 cm^{-1} (H−C≡C bend), where three distinct peaks at low temperature are replaced by a triplet and a doublet at 120 K (Figure 4, second panel). A change in the lattice peak shape accompanies the transition (Figure 4, first panel) as well as shifts in peak shape in the CH_3 s-deform and CH_3 d-deform regions (1300−1500 cm^{-1}; Figure 4, third panel) and the C−C≡C bend region (300−400 cm^{-1}). Although the H−C≡C bend is a key diagnostic band for changes in the propyne crystal structure, this region is not diagnostic across all alkyne ices: it does not demonstrate appreciable change in previously published infrared data of acetylene (ethyne).[31] To our knowledge, no detailed studies of larger alkyne ices have been conducted, so it is yet undetermined if this region is broadly diagnostic for non-symmetric alkynes. Peak positions and assignments are in Table 2 (amorphous propyne, 77 K; crystalline propyne, cooled from 120 to 77 K). Assignments are based on previously published works.[24,32]

Infrared. The infrared spectroscopy temperature series data support the XRD crystalline transition temperature (T_{crys} < 85 K), in contrast with the high crystalline temperature transition that resulted from the Raman experiments (T_{crys} ∼ 105 K). A sharp change is observed in the infrared spectra between 65 and 75 K, which can be ascribed to an amorphous-to-crystalline transition (Figure 5). The most apparent indication is in the 600−750 cm^{-1} region (H−C≡C bend), where a single broad peak at lower temperatures splits into three distinct peaks at and above 75 K. A narrowing and sharpening are also observed for the 3270 cm^{-1} peak (H−C≡ stretch) during the amorphous to crystalline transition. Significant peak wavenumbers and assignments can be found in Table 3 (amorphous propyne, 65 K; crystalline propyne, 75 K). Assignments are based on several previously published works.[25,26,32,33] A full temperature series for IR can be found in Figure S4.

DISCUSSION

X-ray Diffraction. The XRD results indicate that there is only one crystalline phase of propyne observed, consistent with previously published vibrational spectroscopic measurements.[26] Indexing of the synchrotron data suggests that the crystal structure consists of two independent molecules, justified by the calculated density from the volume of the determined unit cell. The general position in the *Pbca* space group has a multiplicity of 8—hence pursuing a structure solution with one molecule would result in an unlikely density

https://doi.org/10.1021/acsearthspacechem.3c00303
ACS Earth Space Chem. 2024, 8, 957−964

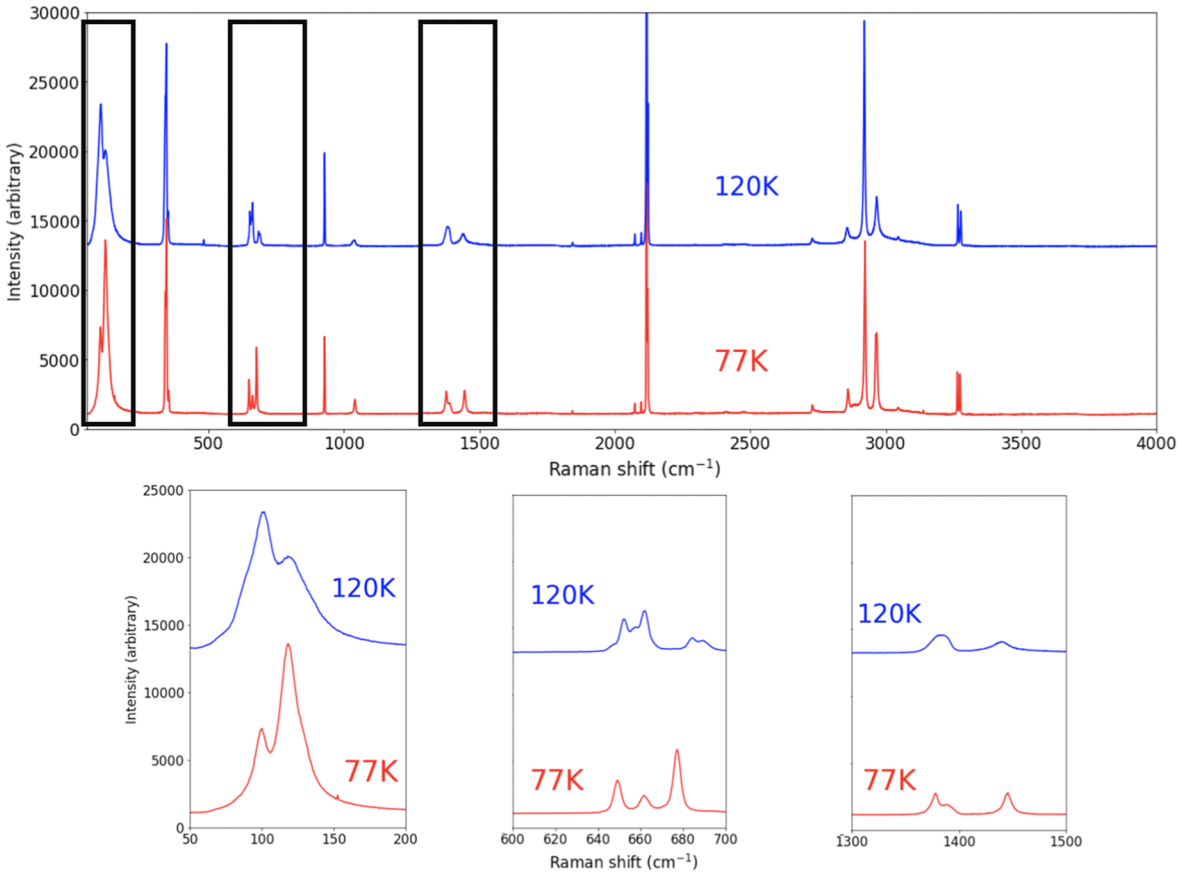

Figure 4. Raman spectra of amorphous phase (red trace; bottom) and crystalline phase (blue trace; top) propyne ice. Expanded views of characteristic spectral regions are highlighted in the bottom panels.

Table 2. Prominent Raman Features of Propyne

	amorphous, 77 K		crystalline, 77 K	
description	wavenumber (cm^{-1})	peak character	wavenumber (cm^{-1})	peak character
lattice	100	doublet	105	doublet
lattice	118	doublet	126	doublet
C−C≡C bend	339	doublet		
C−C≡C bend	343	doublet	343	
H−C≡C bend	649		653	triplet
H−C≡C bend			658	triplet
H−C≡C bend	661		663	triplet
H−C≡C bend	677		686	doublet
H−C≡C bend			693	doublet
C−C str	928		928	
CH_3 rock	1040		1037	
CH_3 s-deform	1378		1379	
CH_3 d-deform	1446		1438	
C≡C stretch	2117	doublet	2117	doublet
C≡C stretch	2122	doublet	2122	doublet
CH_3 s-stretch	2924		2921	
CH_3 d-stretch	2964	doublet		
CH_3 d-stretch	2968	doublet	2967	
H-C≡ stretch	3265		3264	
H-C≡ stretch	3275		3276	

of 441.05 kg m^{-3}. With two molecules each at a general position, the resultant density is 882.10 kg m^{-3}, on par with the behavior of other small organic solids (877.0 kg m^{-3} for butadiene at 90 K[34] and 830 kg m^{-3} for propane at 30 K[35]). A previously published propyne study[26] measured a density of 866 kg m^{-3} at 80 K, a value in very good agreement to that reported here (determined at 90 K). The interpretation of two independent molecules per unit cell is further supported by the obtained Raman spectra (Figure 4), where two peaks are observed for the terminal H−C≡ stretch at 3264 and 3276 cm^{-1} (Table 2), indicating two distinct chemical environments for the propyne molecule in the crystalline solid phase. Using this experimentally determined density, we can recalculate the deposition rate on Titan's surface based on published Titan atmosphere models from 0.23 to 1200 to 0.26−1400 μm/Myr.

While the quality of the powder diffraction data is insufficient to yield a viable crystal structure, the temperature series does indicate significant anisotropy in thermal expansion, with the majority occurring along the *b* axis. The unit cell volume is found to expand by ∼4% over the temperature range between 85 and 160 K. Such anisotropic behavior and magnitude of expansion are on par with the behavior of other small organic solids that have been characterized under Titan-relevant conditions (e.g., butadiene,[34] benzene[36]).

Raman. The unexpectedly high crystalline phase transition temperature is most likely attributed to the high deposition rate of the Raman system. As early as 1951, it has been noted in literature that the rate and temperature of initial condensation of the compound affect the amorphous-to-crystalline temperature transition.[37] Our infrared spectroscopy system is capable of temperatures approximately 60 K lower than the lowest that our Raman spectroscopy system can reach. The rate of deposition in the infrared spectrometer system was 0.075 μm/min, while that in the Raman spectroscopy system is

https://doi.org/10.1021/acsearthspacechem.3c00303
ACS Earth Space Chem. 2024, 8, 957−964

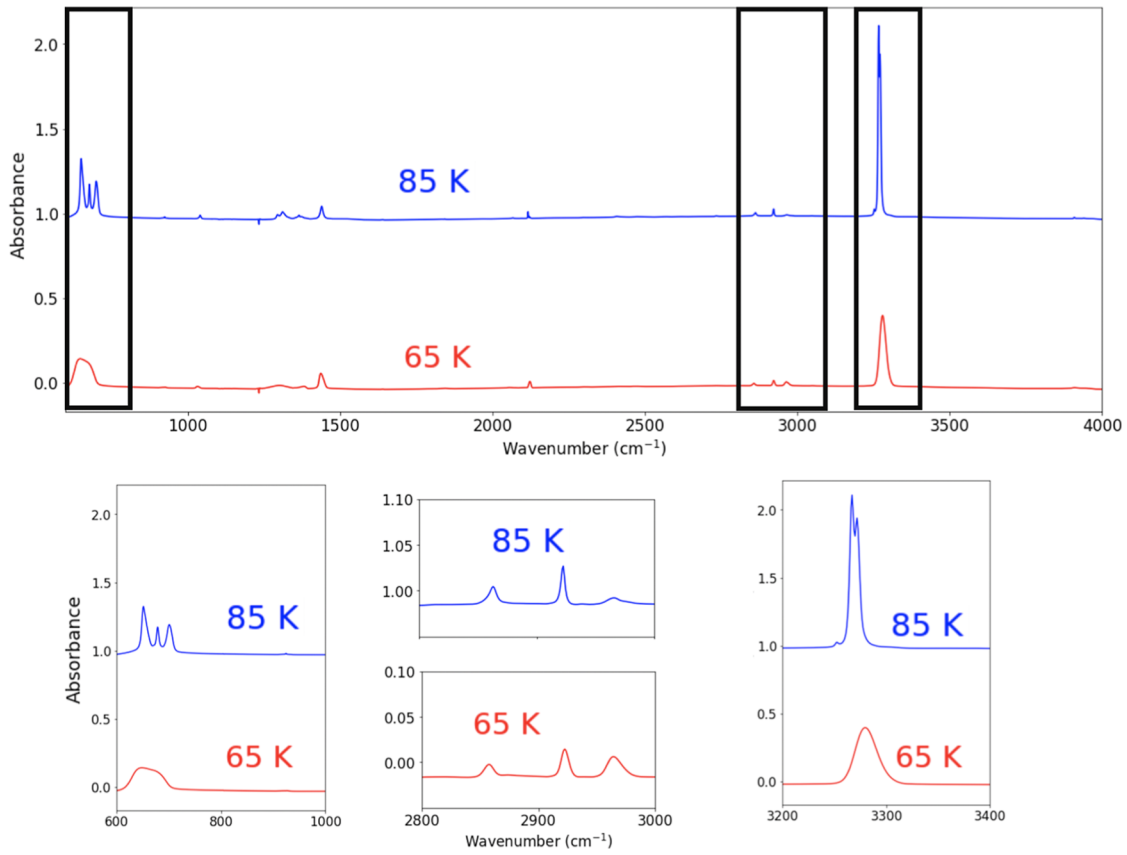

Figure 5. Infrared spectra of the amorphous phase (red trace; bottom) and crystalline (blue trace; top) phase propyne ice. Expanded views of characteristic spectral regions are highlighted in the bottom panels.

Table 3. Prominent IR Features of Propyne and Comparison to Previous Publication

	wavenumber (cm^{-1})			
description	amorphous, 15 K	amorphous, 8 K (Hudson et al.)	crystalline, 75 K	crystalline, 80 K (Hudson et al.)
H−C≡C bend	649	645	651	(not reported)
H−C≡C bend			679	678
H−C≡C bend			701	700
C−H bend	1437	1437	1440	1441
C≡C stretch	2123	2124	2117	2117
H−C≡ stretch			3266	3266
H−C≡ stretch	3279	3280	3271	(not reported)

significantly faster. It seems that the Raman vacuum cryostage is vulnerable to these variations, as the 105 K ice film warmed from 75 K was in mid amorphous-to-crystalline transition, but a direct deposit at 105 K was entirely crystalline.

The 340 cm^{-1} feature seems particularly sensitive to the deposition environment (Figure S2). Although the direct deposition spectral trace (purple; top, deposited at 105 K) is nearly indistinguishable from the crystalline phase observed in the decreasing temperature series (green; middle, deposited at 120 K), the 340 cm^{-1} feature exhibits variation. The direct deposition feature has the primary peak and two pronounced shoulders, while the decreasing temperature feature at this frequency has only one slight shoulder.

Infrared. The observed 75 K crystalline transition temperature, determined from infrared spectroscopy experiments, is consistent with those published by Hudson et al. (2021). Hudson et al. reported that the amorphous-to-crystalline phase change for propyne occurred around 70 K and was completed by 80 K. Note that Hudson et al. did not perform propyne experiments at 75 K. Minor differences in the amorphous-to-crystalline phase change temperatures between our work and that of Hudson et al. can be attributed to variations in deposition and annealing temperatures, deposition rates, and experimental procedures and setups. Our IR spectroscopy results affirm the XRD results that propyne is crystalline at 85 K and reinforces the impact of the fast deposition rate of the Raman experiments, which is the primary cause of the 30 K increase in the observed amorphous-to-crystalline transition temperature of 105 K. We do note that the IR and Raman vacuum system pressures were not identical, which could cause additional [minor] variations among the observed amorphous-to-crystalline transition temperatures.

CONCLUSIONS

We present the first X-ray diffraction and Raman spectroscopy data of propyne ice. From infrared spectroscopy, Raman spectroscopy, X-ray diffraction, and thermal expansion data, it can be concluded that propyne has one solid amorphous phase and one solid crystalline phase, a finding that is in agreement with previous work.[26] From XRD, we conclude that the propyne structure is orthorhombic, with a crystalline transition temperature less than 85 K and a corresponding density of 882.10 kg m^{-3}. This density is consistent with that calculated

https://doi.org/10.1021/acsearthspacechem.3c00303
ACS Earth Space Chem. 2024, 8, 957−964

by Hudson et al. (2021) at 80 K. From the IR spectroscopy experiments, we determined a crystalline transition temperature of 75 K, consistent with that of Hudson et al. (2021). Thus, if pure propyne were to condense in Titan's stratosphere, it would condense in its crystalline phase.

■ ASSOCIATED CONTENT

Supporting Information

The Supporting Information is available free of charge at https://pubs.acs.org/doi/10.1021/acsearthspacechem.3c00303.

Additional temperature series data figures; Raman spectroscopy; and infrared spectroscopy (PDF)

■ AUTHOR INFORMATION

Corresponding Author

Theresa C. Marlin − *NASA Jet Propulsion Laboratory, California Institute of Technology, Pasadena, California 91109, United States; Division of Geological and Planetary Sciences, California Institute of Technology, Pasadena, California 91125, United States;* orcid.org/0009-0003-0670-5474; Email: tmarlin@caltech.edu

Authors

Morgan L. Cable − *NASA Jet Propulsion Laboratory, California Institute of Technology, Pasadena, California 91109, United States;* orcid.org/0000-0002-3680-302X

Tuan H. Vu − *NASA Jet Propulsion Laboratory, California Institute of Technology, Pasadena, California 91109, United States;* orcid.org/0000-0001-6839-9765

Helen E. Maynard-Casely − *Australian Nuclear Science and Technology Organisation, Kirrawee DC, New South Wales 2234, Australia;* orcid.org/0000-0001-6364-9665

Melissa Ugelow − *NASA Goddard Space Flight Center, Greenbelt, Maryland 20771, United States*

Carrie Anderson − *NASA Goddard Space Flight Center, Greenbelt, Maryland 20771, United States*

Robert Hodyss − *NASA Jet Propulsion Laboratory, California Institute of Technology, Pasadena, California 91109, United States*

Complete contact information is available at: https://pubs.acs.org/10.1021/acsearthspacechem.3c00303

Author Contributions

The manuscript was written through contributions of all authors. All authors have approved the final version of the manuscript.

Funding

T.C.M. was funded by NSF GRFP. All other authors were funded by a Cassini Data Analysis Program grant.

Notes

The authors declare no competing financial interest.

■ ACKNOWLEDGMENTS

This work was conducted at the Jet Propulsion Laboratory, California Institute of Technology, under a contract with the National Aeronautics and Space Administration (80NM0018D0004). Reference herein to any specific commercial product, process, or service by trade name, trademark, manufacturer, or otherwise does not constitute or imply its endorsement by the United States Government or the Jet Propulsion Laboratory, California Institute of Technology. T.C.M. was funded by NSF GRFP. All other authors were funded by a Cassini Data Analysis Program grant. This research used resources of the Advanced Photon Source, a U.S. Department of Energy (DOE) Office of Science user facility operated for the DOE Office of Science by Argonne National Laboratory under Contract no. DE-AC02-06CH11357.

■ ABBREVIATIONS

ALMA, Atacama Large Millimeter/submillimeter Array; CIRS, Composite InfraRed Spectrometer; XRD, X-ray Diffraction

■ REFERENCES

(1) Hörst, S. M. Titan's Atmosphere and Climate. *J. Geophys. Res.: Planets* **2017**, *122* (3), 432−482.

(2) Vuitton, V.; Yelle, R. V.; Klippenstein, S. J.; Hörst, S. M.; Lavvas, P. Simulating the Density of Organic Species in the Atmosphere of Titan with a Coupled Ion-Neutral Photochemical Model. *Icarus* **2019**, *324*, 120−197.

(3) Cable, M. L.; Runčevski, T.; Maynard-Casely, H. E.; Vu, T. H.; Hodyss, R. Titan in a Test Tube: Organic Co-Crystals and Implications for Titan Mineralogy. *Acc. Chem. Res.* **2021**, *54* (15), 3050−3059.

(4) Vuitton, V.; Dutuit, O.; Smith, M. A.; Balucani, N. Chemistry of Titan's Atmosphere. In *Titan*; Müller-Wodarg, I., Griffith, C. A., Lellouch, E., Cravens, T. E., Eds.; Cambridge University Press, 2014; pp 224−284..

(5) Maguire, W. C.; Hanel, R. A.; Jennings, D. E.; Kunde, V. G.; Samuelson, R. E. C3H8 and C3H4 in Titan's Atmosphere. *Nature* **1981**, *292* (5825), 683−686.

(6) Teanby, N. A.; Irwin, P. G. J.; Nixon, C. A.; de Kok, R.; Vinatier, S.; Coustenis, A.; Sefton-Nash, E.; Calcutt, S. B.; Flasar, F. M. Active Upper-Atmosphere Chemistry and Dynamics from Polar Circulation Reversal on Titan. *Nature* **2012**, *491* (7426), 732−735.

(7) Mathé, C.; Vinatier, S.; Bézard, B.; Lebonnois, S.; Gorius, N.; Jennings, D. E.; Mamoutkine, A.; Guandique, E.; Vatant d'Ollone, J. Seasonal Changes in the Middle Atmosphere of Titan from Cassini/CIRS Observations: Temperature and Trace Species Abundance Profiles from 2004 to 2017. *Icarus* **2020**, *344*, 113547.

(8) Teanby, N. A.; Irwin, P. G. J.; de Kok, R.; Jolly, A.; Bézard, B.; Nixon, C. A.; Calcutt, S. B. Titan's Stratospheric C2N2, C3H4, and C4H2 Abundances from Cassini/CIRS Far-Infrared Spectra. *Icarus* **2009**, *202* (2), 620−631.

(9) Cordiner, M. A.; Palmer, M. Y.; Nixon, C. A.; Irwin, P. G. J.; Teanby, N. A.; Charnley, S. B.; Mumma, M. J.; Kisiel, Z.; Serigano, J.; Kuan, Y.-J.; Chuang, Y.-L.; Wang, K.-S. Ethyl Cyanide on Titan: Spectroscopic Detection and Mapping Using ALMA. *Astrophys. J., Lett.* **2015**, *800* (1), L14.

(10) Coustenis, A.; Jennings, D. E.; Achterberg, R. K.; Bampasidis, G.; Lavvas, P.; Nixon, C. A.; Teanby, N. A.; Anderson, C. M.; Cottini, V.; Flasar, F. M. Titan's Temporal Evolution in Stratospheric Trace Gases near the Poles. *Icarus* **2016**, *270*, 409−420.

(11) Thelen, A. E.; Nixon, C. A.; Chanover, N. J.; Cordiner, M. A.; Molter, E. M.; Teanby, N. A.; Irwin, P. G. J.; Serigano, J.; Charnley, S. B. Abundance Measurements of Titan's Stratospheric HCN, HC3N, C3H4, and CH3CN from ALMA Observations. *Icarus* **2019**, *319*, 417−432.

(12) Coustenis, A.; Jennings, D. E.; Achterberg, R. K.; Bampasidis, G.; Nixon, C. A.; Lavvas, P.; Cottini, V.; Flasar, F. M. Seasonal Evolution of Titan's Stratosphere Near the Poles. *Astrophys. J., Lett.* **2018**, *854* (2), L30.

(13) Sylvestre, M.; Teanby, N. A.; Vinatier, S.; Lebonnois, S.; Irwin, P. G. J. Seasonal Evolution of C2N2, C3H4, and C4H2 Abundances in Titan's Lower Stratosphere. *Astron. Astrophys.* **2018**, *609*, A64.

(14) Lombardo, N. A.; Nixon, C. A.; Achterberg, R. K.; Jolly, A.; Sung, K.; Irwin, P. G. J.; Flasar, F. M. Spatial and seasonal variations

in C3Hx hydrocarbon abundance in Titan's stratosphere from Cassini CIRS observations. *Icarus* **2019**, *317*, 454−469.
(15) Vinatier, S.; Bézard, B.; Lebonnois, S.; Teanby, N. A.; Achterberg, R. K.; Gorius, N.; Mamoutkine, A.; Guandique, E.; Jolly, A.; Jennings, D. E.; Flasar, F. M. Seasonal Variations in Titan's Middle Atmosphere during the Northern Spring Derived from Cassini/CIRS Observations. *Icarus* **2015**, *250*, 95−115.
(16) Anderson, C. M.; Samuelson, R. E.; Nna-Mvondo, D. Organic Ices in Titan's Stratosphere. *Space Sci. Rev.* **2018**, *214* (8), 125.
(17) Krasnopolsky, V. A. A Photochemical Model of Titan's Atmosphere and Ionosphere. *Icarus* **2009**, *201* (1), 226−256.
(18) Lara, L. M.; Lellouch, E.; López-Moreno, J. J.; Rodrigo, R. Vertical Distribution of Titan's Atmospheric Neutral Constituents. *J. Geophys. Res.: Planets* **1996**, *101* (E10), 23261−23283.
(19) Yung, Y. L.; Allen, M.; Pinto, J. P. Photochemistry of the Atmosphere of Titan: Comparison between Model and Observations. *Astrophys. J., Suppl. Ser.* **1984**, *55* (3), 465−506.
(20) Cable, M. L.; Vu, T. H.; Malaska, M. J.; Maynard-Casely, H. E.; Choukroun, M.; Hodyss, R. Properties and Behavior of the Acetonitrile-Acetylene Co-Crystal under Titan Surface Conditions. *ACS Earth Space Chem.* **2020**, *4* (8), 1375−1385.
(21) Cable, M. L.; Vu, T. H.; Malaska, M. J.; Maynard-Casely, H. E.; Choukroun, M.; Hodyss, R. A Co-Crystal between Acetylene and Butane: A Potentially Ubiquitous Molecular Mineral on Titan. *ACS Earth Space Chem.* **2019**, *3*, 2808−2815.
(22) Maynard-Casely, H. E.; Hodyss, R.; Cable, M. L.; Vu, T. H.; Rahm, M. A Co-Crystal between Benzene and Ethane: A Potential Evaporite Material for Saturn's Moon Titan. *IUCrJ* **2016**, *3* (3), 192−199.
(23) Cable, M. L.; Vu, T. H.; Maynard-Casely, H. E.; Choukroun, M.; Hodyss, R. The Acetylene-Ammonia Co-Crystal on Titan. *ACS Earth Space Chem.* **2018**, *2* (4), 366−375.
(24) Kalasinsky, V. F.; Little, T. S. Raman Spectra and Vibrational Dephasing of Methylacetylene. *J. Raman Spectrosc.* **1983**, *14* (4), 253−258.
(25) Crawford, B. L. Infra-Red and Raman Spectra of Polyatomic Molecules XII. Methyl Acetylene. *J. Chem. Phys.* **1940**, *8* (7), 526−531.
(26) Hudson, R. L.; Gerakines, P. A.; Yarnall, Y. Y.; Coones, R. T. Infrared Spectra and Optical Constants of Astronomical Ices: III. Propane, Propylene, and Propyne. *Icarus* **2021**, *354*, 114033.
(27) Coelho, A. A. TOPAS and TOPAS-Academic: An Optimization Program Integrating Computer Algebra and Crystallographic Objects Written in C++. *J. Appl. Crystallogr.* **2018**, *51* (1), 210−218.
(28) Mahjoub, A.; Hodyss, R. Thermal Reaction in Cometary and Pre-Cometary Ices: Formation of Thiocarbamate in OCS-CH3NH2 Mixed Ices. *Astrophys. J.* **2018**, *869* (2), 98.
(29) Johnson, P. V.; Markus, C. R.; Hodyss, R. Photochemistry of Ozone-Water Ices. *ACS Earth Space Chem.* **2019**, *3* (11), 2430−2436.
(30) Hodyss, R.; Johnson, P. V.; Meckler, S. M.; Fayolle, E. C. Ultraviolet Spectroscopy and Photochemistry of SO2/H2O Ices. *ACS Earth Space Chem.* **2019**, *3* (4), 663−668.
(31) Hudson, R. L.; Ferrante, R. F.; Moore, M. H. Infrared Spectra and Optical Constants of Astronomical Ices: I. Amorphous and Crystalline Acetylene. *Icarus* **2014**, *228*, 276−287.
(32) Shimanouchi, T. *Tables of Molecular Vibrational Frequencies Consolidated Volume I*; National Bureau of Standards, 1972; pp 1−160.
(33) Whitmer, J. C. Normal Coordinates and Potential Energy Distributions of Methyl Acetylene and Some Halogen Substituted Analogues. *J. Mol. Struct.* **1974**, *21*, 173.
(34) Vu, T. H.; Maynard-Casely, H. E.; Cable, M. L.; Choukroun, M.; Malaska, M. J.; Hodyss, R. 1,3-Butadiene on Titan: Crystal Structure, Thermal Expansivity, and Raman Signatures. *ACS Earth Space Chem.* **2022**, *6* (10), 2274−2281.
(35) Boese, R.; Weiss, H.-C.; Bläser, D. The Melting Point Alternation in the Short-Chain n-Alkanes: Single-Crystal X-Ray Analyses of Propane at 30 K and of n-Butane to n-Nonane at 90 K. *Angew. Chem., Int. Ed.* **1999**, *38* (7), 988−992.
(36) Czaplinski, E.; Yu, X.; Dzurilla, K.; Chevrier, V. Experimental Investigation of the Acetylene-Benzene Cocrystal on Titan. *Planet. Sci. J.* **2020**, *1* (3), 76.
(37) Malherbe, F. E.; Bernstein, H. J. Infrared Spectra of Rapidly Solidified Vapors. *J. Chem. Phys.* **1951**, *19* (12), 1607−1608.

https://doi.org/10.1021/acsearthspacechem.3c00303
ACS Earth Space Chem. 2024, 8, 957−964